Computer Networks 234 (2023) 109922

Contents lists available at ScienceDirect

Computer Networks

journal homepage: www.elsevier.com/locate/comnet

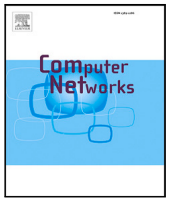

Open-access millimeter-wave software-defined radios in the PAWR COSMOS testbed: Design, deployment, and experimentation ☆

Tingjun Chen [a,*], Prasanthi Maddala [b], Panagiotis Skrimponis [c], Jakub Kolodziejski [b], Abhishek Adhikari [d], Hang Hu [e], Zhihui Gao [a], Arun Paidimarri [f], Alberto Valdes-Garcia [f], Myung Lee [e], Sundeep Rangan [c], Gil Zussman [d], Ivan Seskar [b]

[a] Electrical and Computer Engineering, Duke University, Durham, NC, USA
[b] WINLAB, Rutgers University, North Brunswick, NJ, USA
[c] Electrical and Computer Engineering, NYU, Brooklyn, NJ, USA
[d] Electrical Engineering, Columbia University, New York, NY, USA
[e] Electrical Engineering, The City College of New York, New York, NY, USA
[f] IBM Research, Yorktown Heights, NY, USA

ARTICLE INFO

Dataset link: https://wiki.cosmos-lab.org/wiki/

Keywords:
Millimeter-wave communication
Software-defined radios
Wireless experimentation
COSMOS testbed

ABSTRACT

While millimeter-wave (mmWave) wireless has recently gained tremendous attention with the transition to 5G, developing a broadly accessible experimental infrastructure will largely facilitate the research and allow the community to make significant progress in this area. In this paper, we present the design and implementation of various programmable and open-access mmWave software-defined radios (SDRs) that have been deployed in the PAWR COSMOS advanced wireless testbed, in both indoor and outdoor environments. These programmable mmWave radios are based on the IBM 28 GHz 64-element dual-polarized phased array antenna module (PAAM) subsystem board and the Sivers IMA 60 GHz WiGig transceiver. These front ends are integrated with USRP SDRs or Xilinx RFSoC boards, which provide baseband signal processing capabilities. Moreover, we present measurements of the TX/RX beamforming performance and example experiments (e.g., real-time channel sounding and RFNoC-based 802.11ad preamble detection), using the mmWave radios. Finally, we discuss ongoing enhancement and development efforts focusing on these radios.

1. Introduction

Millimeter-wave (mmWave) communication is a key technology for 5G and future wireless networks, where the widely available spectrum at mmWave frequencies can be leveraged to achieve very high data rates (above Gbps) in cellular, Wi-Fi, and wireless backhaul systems [1–4]. Such capabilities can enable a broad range of real-time applications including autonomous vehicles, augmented reality, and smart cities. While there has been extensive recent development and demonstrations of practical mmWave systems (e.g., [5–10]), experimentation with state-of-the-art programmable mmWave radios in real-world environments it still a major challenge for researchers from both academia and industry.

To address this challenge and to allow the broader community to conduct experiments with mmWave wireless and other state-of-the-art technologies, in [11], we presented the design and deployment of the city-scale open-access COSMOS testbed. The COSMOS testbed is being deployed in West Harlem, New York City (NYC), as part of the NSF Platforms for Advanced Wireless Research (PAWR) program [12]. It integrates cutting-edge technologies and hardware across the wireless, optical, and edge cloud domains, and supports experimentation with these technologies in a dense urban environment. One key technological component of the COSMOS testbed is a variety of *programmable* mmWave front ends at 28/60 GHz, USRP software-defined radios (SDRs), and Xilinx RFSoC evaluation boards, as well as end-to-end mmWave systems. These mmWave radios can enable various experimental capabilities across the Physical (PHY), medium access control (MAC), and higher layers of the network stack.

In this paper, we first present an overview of the relevant COSMOS testbed components, including the two sandboxes (`sb1` and `sb2`) and the outdoor testbed (`bed`). Then, we present the programmable

☆ A preliminary version of this paper was presented at the 15th ACM Workshop on Wireless Network Testbeds, Experimental Evaluation & Characterization (WiNTECH'21), Apr. 2022 (Chen et al., 2022).

* Corresponding author.
E-mail address: tingjun.chen@duke.edu (T. Chen).

https://doi.org/10.1016/j.comnet.2023.109922
Received 15 May 2023; Received in revised form 6 July 2023; Accepted 7 July 2023
Available online 13 July 2023

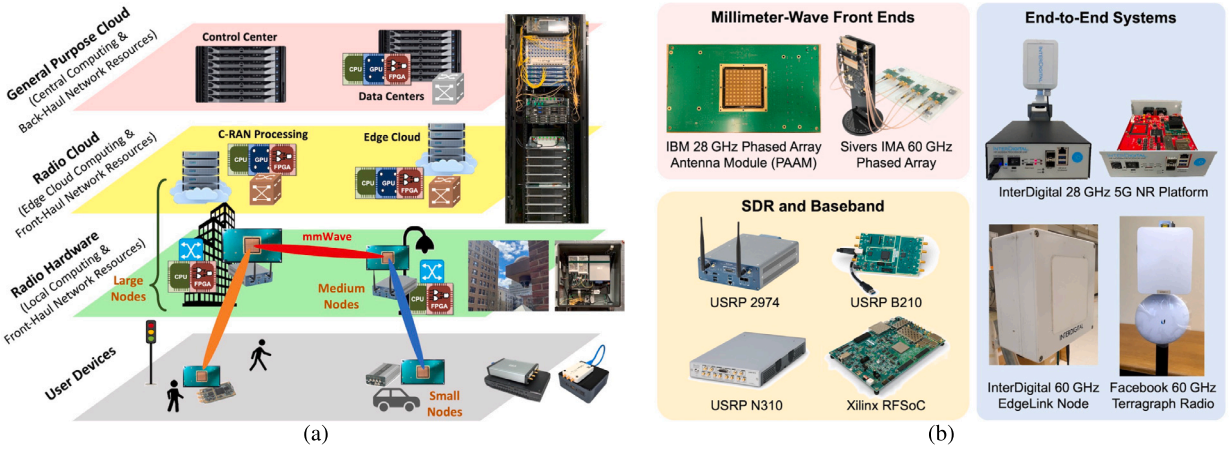

Fig. 1. (a) COSMOS' multi-layered computing architecture, which includes radio nodes with different form factors and computational capabilities, and (b) various millimeter-wave (mmWave) front ends and systems integrated in the COSMOS testbed and sandboxes.

mmWave front ends and their integration with USRP SDRs and/or Xilinx RFSoC boards, which have been deployed in the COSMOS testbed. These front ends include the IBM 28 GHz 64-element dual-polarized phased array antenna module (PAAM) subsystem board presented in [13,14], which integrates a 28 GHz PAAM [15,16], and the Sivers IMA 60 GHz WiGig transceiver system. In particular, the indoor sandboxes include a number of programmable 28/60 GHz radios mounted on fixed tripods and an X-Y positioning table. The outdoor testbed, located in an FCC Innovation Zone [17], features a number of programmable 28 GHz radios as part of wall-mounted infrastructure nodes. We also present the developed software and application program interfaces (APIs) for hardware control and experimentation. Finally, we present extensive measurements and experiments with the IBM 28 GHz PAAM subsystem board, which is integrated with a USRP N310 SDR, and the Sivers IMA 60 GHz transceiver, which is integrated with a USRP N310 SDR and a Xilinx RFSoC board. The developed example experiments and measurement datasets are publicly available at [18,19]. Other experiments that can be supported by COSMOS' programmable sub-6 GHz/mmWave radios include but are not limited to dynamic spectrum access and sharing/coexistence [20], channel sounding and beam tracking [21], and full-duplex wireless [22,23].

To summarize, this paper details the design and implementation of the programmable and open-access 28/60 GHz radios, which are deployed in real-world indoor and outdoor environments and can be remotely used by the community. These open-access hardware and software resources together with a suite of example experiments can be extended to more complicated networking scenarios, therefore facilitating experimentation with advanced mmWave technologies. The rest of the paper is organized as follows. We review related work in Section 2. We present an overview of the PAWR COSMOS testbed and its programmable mmWave radios in Sections 3 and 4. Then, we present extensive measurements and experiments using COSMOS' mmWave radios in Sections 5 and 6, followed by the conclusion in Section 7.

2. Related work

mmWave communications and networking: Various channel measurement campaigns in different mmWave frequency bands and in different environments (e.g., [1,24,25]). Recent works demonstrated the feasibility of mmWave links supported and focused on beam-tracking, beam-alignment, and beam-steering methods (e.g. [26–28]), and improving the robustness of mmWave links under mobility and blockage was studied [29–31]. mmWave MIMO has been studied in both theoretical and experimental contexts (see [32] and the references therein). For example, [33] presents a MIMO beam-steering scheme leveraging the mmWave channel sparsity, and [6] presents the design of a MIMO mmWave software radio.

mmWave systems and platforms: In addition, there have been extensive efforts on the design and development of practical mmWave systems and testbeds, including the X60 platform [5], M-Cube [6], mmFLEX [7], MIMORPH [8], Pi-Radio [34], OpenMili [9], and MiRa [10], which mostly focus on 60 GHz wireless. In particular, X60 [5] is an SDR-based testbed for 60 GHz WLANs using a small 12-element phased antenna array with programmable PHY, MAC, and network layers. M-Cube [6] is a 60 GHz massive MIMO SDR based on the commodity Airfide IEEE 802.11ad radio. The most relevant to COSMOS' 60 GHz SDRs is MIMORPH [8], which is a real-time experimental platform for sub-6 GHz and mmWave MIMO systems, where the Sivers IMA 60 GHz transceiver is integrated with a Xilinx RFSoC board.

Other PAWR testbeds: Across the other PAWR testbeds [12], the POWDER-RENEW [35,36] testbed builds a flexible infrastructure enabling a wide range of software-defined experiments including massive MIMO, O-RAN, and spectrum sharing. The AERPAW [37] testbed has a technological focus on studying the convergence of 5G technology and autonomous drones. The ARA testbed [38] focuses on building a wireless living lab for smart and connected rural communities, as well as research and development of rural-focused wireless technologies and applications. The Colosseum testbed [39] is a large-scale RF emulator designed to support the research and development of next-generation radio network technologies in a repeatable and highly configurable RF environment.

In this paper, we focus on the COSMOS testbed that provides a broad range of programmable and open-access mmWave front ends deployed in a dense urban setting in West Harlem, NYC. These mmWave front ends with more advanced capabilities include the IBM 28 GHz PAAM subsystem board, whose integration with an SDR and an API as a software-defined phased array platform was described in [40]. We also reported extensive 28 GHz channel measurement and propagation modeling in the COSMOS testbed area in [24,41], which help drive the deployment of the 28 GHz SDRs in the COSMOS testbed. Other key technological focuses of COSMOS include programmable optical x-haul networking [42] and edge cloud computing for smart city applications [11].

3. The PAWR COSMOS testbed

COSMOS [11,43] is an open-access city-scale advanced wireless testbed that is being deployed in West Harlem, NYC, as part of the NSF

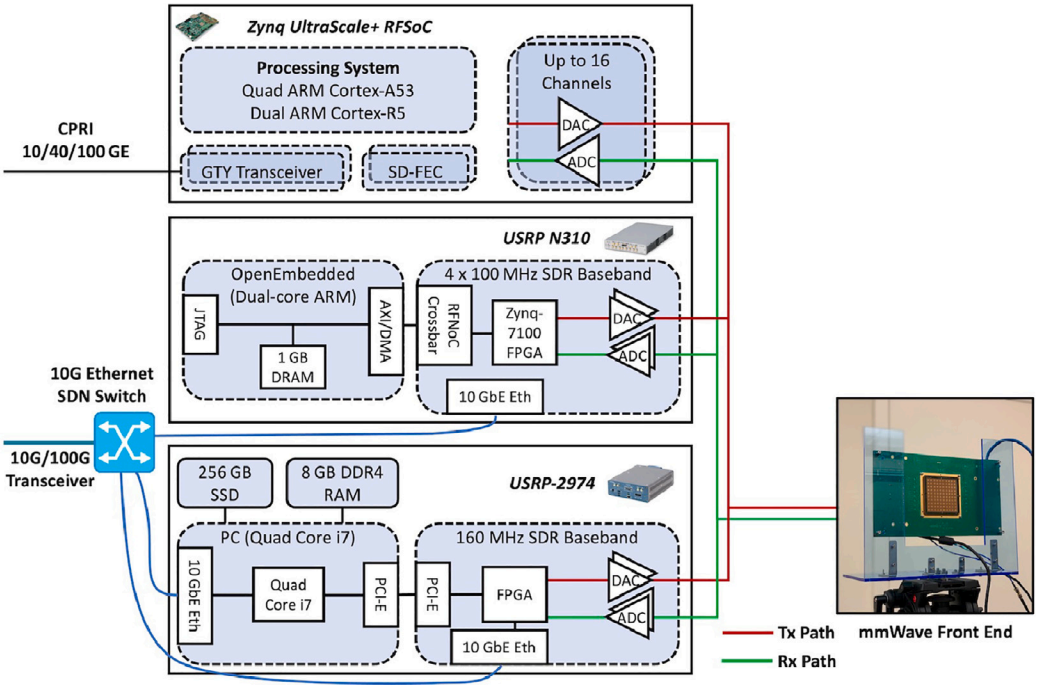

Fig. 2. Example block diagram of a programmable mmWave node in COSMOS, where different configurations include a subset of the major components (e.g., the 28 GHz PAAM board with a USRP N310).

PAWR program [12]. Fig. 1(a) shows COSMOS' multi-layered computing and network architecture with different levels of programmability from user devices up to the edge and central cloud. In particular, there are three types of COSMOS nodes with different form factors for different deployment scenarios, which include: *large* nodes (macro cells installed on rooftops), *medium* nodes (small cells installed on building side and lightpoles), and *small* nodes (near-portable fixed or mobile devices). The deployment of COSMOS consists of three main sites:

(*i*) A sandbox located in WINLAB at Rutgers University with both indoor and outdoor deployments (sb1);
(*ii*) An indoor sandbox located in the CEPSR Building at Columbia University (sb2); and
(*iii*) The outdoor testbed site (bed) that is currently being deployed in West Harlem, NYC, around the Columbia University and City College of New York (CCNY) campuses.

The open-access nature of COSMOS allows worldwide users to remotely use the testbed and experiment with advanced wireless, optical, and edge cloud technologies. More details about the architecture design and deployment of the COSMOS testbed, as well as datasets collected using the testbed (e.g., extensive 28 GHz channel measurements in the testbed area) can be found in [11,13,24,41–43].

Key technological components of the COSMOS testbed are several mmWave front end systems and radios, as shown in Fig. 1(b) and described in Section 4. In particular, COSMOS includes two main mmWave front end systems: (*i*) the IBM 28 GHz 64-element dual-polarized phased array antenna module (PAAM) subsystem board (Section 4.1), and (*ii*) the Sivers IMA 60 GHz 16-element phased array transceiver (Section 4.2), each of which can be attached to an SDR or a Xilinx RFSoC board to form a *programmable* mmWave radio (Sections 4.3 and 4.4). Fig. 2 shows an example diagram of a COSMOS node equipped with mmWave capabilities, which includes a mmWave front end system (e.g., the 28 GHz PAAM board) and an SDR (e.g., the USRP N310). It also shows the mounting structure and wall-mounted enclosures for node electronics and antennas for indoor and outdoor deployments, respectively (Sections 4.5 and 4.6). Different SDRs and compute hosts are selected based on the node form factor and portability requirements. For example, an infrastructure medium node mounted on a building side with available power supply consists of a high-end USRP N310 SDR connected to the compute servers via a high-speed optical front-haul, whereas a mobile node consists of a USRP 2974 SDR with an embedded PC for data storage and processing (Section 4.7).

COSMOS also supports end-to-end mmWave experimentation using the 28 GHz 5G NR platform and 60 GHz EdgeLink nodes from InterDigital (Section 4.5), and the 60 GHz Terragraph radios from Facebook as part of the Telecom Infra Project (TIP). In this paper, we focus on the programmable mmWave front ends integrated with SDRs. More detailed information about these end-to-end systems and the relevant tutorials are available at [18,19].

4. Programmable mmwave radios in the COSMOS testbed

In this section, we present programmable mmWave radios in the COSMOS testbed and focus on the 28 GHz and 60 GHz SDRs based on the IBM 28 GHz PAAM subsystem board and the Sivers IMA 60 GHz WiGig transceiver, respectively. We also present the deployments of these mmWave radios in both indoor sandboxes (sb1 and sb2) and outdoor environments (bed).

4.1. IBM 28 GHz PAAM subsystem board

Fig. 3(a) shows the IBM 28 GHz 64-element dual-polarized PAAM [15,16], which can enable a broad range of mmWave experiments with multi-beam support and fast (e.g., sub-μs) beam steering capability. An important feature of the PAAM is the use of antenna feed lines with equal delay, uniform antenna radiation patterns across the array, and orthogonal amplitude and phase control per element in the IC, which enable high-precision beam steering capability *without any calibration*. Fig. 3(b) shows the architecture diagram of a compact 28 GHz *PAAM subsystem board* reported in [14], which is a 10 in×5.75 in printed circuit board (PCB) consisting of a 28 GHz PAAM, intermediate frequency (IF) and local oscillator (LO) splitters, IF/LO baluns, programmable switches, and an on-board phased locked loop (PLL) for LO generation. The detailed 28 GHz PAAM subsystem architecture as well as the software and firmware control architecture can be found in [14].

The TX/RX interfaces of the PAAM board are at 3 GHz IF through SMP connectors, which allows for direct connection to a USRP SDR

Table 1
Main board-level and IC-level functions supported by the PAAM subsystem board and software API.

PAAM API command	Function
Board-level functions for the PAAM subsystem board object, paam_board	
paam_board.set_lo_switch(bool external)	Set the LO switch to use an external LO source or the on-board PLL
paam_board.pll_init()	Initialize and set the on-board PLL (use only with function set_lo_switch(external=False))
paam_board.set_if_tx_h(bool combine)	Set the IF TX input in H-polarization to combined (across 4 ICs) or separate (individual IC)
paam_board.set_if_tx_v(bool combine)	Set the IF TX input in V-polarization to combined (across 4 ICs) or separate (individual IC)
paam_board.set_if_rx_h(bool combine)	Set the IF RX output in H-polarization to combined (across 4 ICs) or separate (individual IC)
paam_board.set_if_rx_v(bool combine)	Set the IF RX output in V-polarization to combined (across 4 ICs) or separate (individual IC)
paam_board.get_adc_vals()	Read values from the 12 ADC channels including the current consumption of individual ICs and the entire PAAM board
IC-level functions for the PAAM object, paam	
paam.enable(ic, fe_list, txrx, pol)	Enable and configure a set of front end elements (fe_list) for a given IC (ic), TX/RX mode (txrx), and polarization (pol)
paam.steer_beam(ics, txrx, pol, theta, phi)	Steer the beam to a given direction (theta, phi) for a given set of ICs (ics), TX/RX mode (txrx), and polarization (pol). Across the TX-H, TX-V, RX-H, and RX-V configurations, up to 770 entries for 64-element beams can be stored in the on-chip beam table, and this number increases for 16-element beams
paam.set_arbitrary_beam(ics, txrx, pol, gains, phases)	Set arbitrary beam patterns by setting the phase and gain for each individual front end element
paam.switch_beam_index(ic, txrx, pol, beam_index)	Switch to the pre-recorded beam index (beam_index) for a given IC (ic), TX/RX mode (txrx), and polarization (pol). For each of the TX-H, TX-V, RX-H, and RX-V configurations, 128 entries can be stored in the on-chip beam table
paam.switch_beam_indexes(ic, txrx, beam_index_h, beam_index_h)	Switch to the pre-recorded beam indexes in both H-polarization and V-polarization simultaneously (beam_index_h and beam_index_v) for a given IC (ic) and TX/RX mode (txrx)

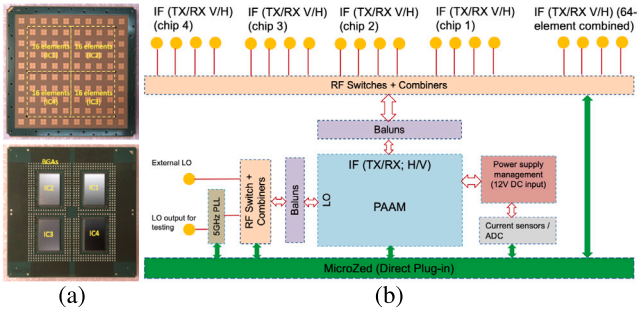

Fig. 3. (a) Top and bottom views of an IBM 28 GHz PAAM [15], (b) architecture diagram of the 28 GHz PAAM subsystem board [14].

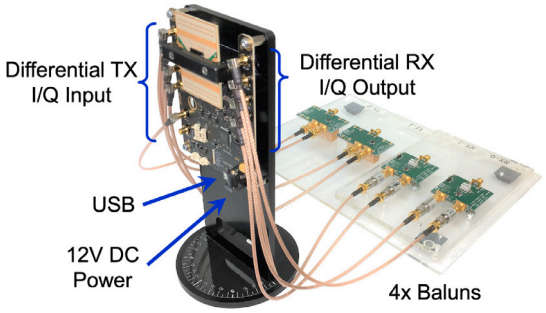

Fig. 4. The Sivers IMA 60 GHz WiGig transceiver with baluns.

or an RFSoC board. We prototyped four 28 GHz SDRs using the PAAM boards and N310 SDRs in sb1 and sb2, as shown in Figs. 5 and 7. Using the IF switches/splitters and the 20 IF ports on the PAAM subsystem board, a broad range of SISO and MIMO mmWave configurations can be realized. These include, for instance, up to 8 simultaneous 16-element independent beams or up to 2 simultaneous 64-element independent beams in each TX/RX mode across both H- and V-polarization. The PAAM subsystem board also supports the direct plug-in of an off-the-shelf Avnet MicroZed FPGA system-on-module. The MicroZed FPGA and associated software enable the configuration of all subsystem features from a high-level API. Further details about the development of the 28 GHz PAAM subsystem board are in [14].

The software and firmware control architecture of the developed 28 GHz PAAM board are presented in [14]. This architecture evolved from the software-define phased array radio (SDPAR) demonstration presented in [40]. In particular, users can send high-level PAAM control commands from the host to the MicroZed FGPA via the Ethernet interface using the Python-based API. When the ARM processor core of the MicroZed FPGA receives the commands, it will initiate the low-level communication protocols to communicate with and configure the PAAM subsystem board. Table 1 summarizes the main board-level and IC-level functions supported by the PAAM board and the software API, which are responsible for configuring the PAAM subsystem board (e.g., PLL for on-board LO generation and IF switches) and the PAAM itself (e.g., TX/RX mode of operation, H/V-polarization, number of activated front end elements, and control of beamforming). In Section 5, we present measurements and example experiments using the PAAM boards integrated with USRP N310 SDRs, using the developed API.

4.2. Sivers IMA 60 GHz WiGig transceiver

Another mmWave front end supported by COSMOS is the Sivers IMA 57–66 GHz WiGig transceiver system, which is optimized for high-performance WiGig applications and is compliant with the IEEE 802.11ad standard. This transceiver, which was also used in [7,8], includes two integrated 16-element patch antenna arrays for TX and RX, and supports beam steering capabilities using an application GUI or a Python API over the USB interface. We connect the Sivers IMA transceiver with COTS baluns to convert its differential TX input and RX output ports to single-ended ports, as shown in Fig. 4, which are further connected to a USRP SDR or a Xilinx RFSoC board to form a programmable 60 GHz SDR. In Section 6, we present experimentation with the Sivers 60 GHz transceiver with both a USRP N310 SDR and a Xilinx RFSoC board, using the setup shown in Fig. 5.

4.3. USRP SDRs and RFNoC

In general, SDRs are used for baseband processing for radios operating in both sub-6 GHz and mmWave frequency bands. COSMOS' programmable mmWave radios use a range of USRP SDRs (including the USRP-2974, N310, and B210) for high-bandwidth data streaming and processing. In particular, the USRP-2974 and N310 SDRs are equipped with on-board CPUs and can be used in stand-alone mode or in conjunction with a host server. The 10 GbE SFP+ ports on the USRP-2974 and N310 are connected to COSMOS' data networks, allowing for high-speed data transfer between the SDR and host server. For real-time experimentation, we exploit the USRP hardware driver (UHD), which is targeted mainly at USRP devices.

Many USRP SDRs, including the USRP-2974 and N310, support the RFNoC development framework, which leverages the resource-dense FPGAs with each SDR for real-time signal processing. RFNoC is a unique processing and routing architecture for 3rd-generation USRP devices, which reduces the FPGA development time by providing basic SDR functionalities (e.g., host communication, radio interfaces, and clocking) while allowing users to easily integrate custom IP. It also allows for dynamic composition of flowgraphs by connecting various FPGA modules at run-time. Attaching mmWave front ends to RFNoC-enabled USRP SDRs in COSMOS allows users to offload computationally intensive and time-sensitive tasks to the FPGA in a mixed hardware-software design.

4.4. Xilinx RFSoC ZCU111 boards

COSMOS's mmWave radios also leverage the Xilinx RFSoC boards as another SDR platform for high-bandwidth data streaming and processing. The core processing of an RFSoC-based SDR is a ZCU111 evaluation board featuring a Xilinx Zynq UltraScale+ ZU28DR RFSoC FPGA, a quad-core ARM Cortex-A53 processing system and a dual-core ARM Cortex-R5 real-time processor, 8 high-speed 14-bit DACs and 12-bit ADCs, and several high-speed gigabit transceiver ports. Another highlight of this board is the soft-decision forward error correction (SD-FEC) cores in silicon, which are used to implement highly computational codes (e.g., Turbo, LDPC, and Polar codes) without using any FPGA resources.

Similarly to the USRP SDRs, the ZCU111 board is also addressable through a 1 GbE connection and allows for access to the embedded Linux system. The host can access the ZCU111 board through a network RPC-based API and communicate with the module peripheral manager daemon. For applications requiring high data rates, four 10 GHz SFP+ interfaces on the ZCU111 board can be used. Using the Xilinx Vivado tool and open-embedded Linux tools, we modified the open-source files of UHD 3.13 to target the ZCU111 board. Such a unified software interface allows seamless transition between different applications, and any software supporting a UHD device (i.e., GNU Radio) can be used to control the ZCU111 board.

For non-real-time experimentation, the ZCU111 board is connected to a host server via the 1/10/25 GbE interface over TCP/IP. The host drivers are implemented in both Python and MATLAB, enabling a wide range of experiments. The TX data can be generated and prestored in the block random access memory (BRAM), and the RX data can be collected in continuous or burst mode and stored in the PL-DDR memory integrated within the programmable logic fabric for post processing. The user can also define the number of FPGA clock cycles (@491.52 MHz) to pause between measurements.

For RF front ends supporting multiple channels such as the IBM 28 GHz PAAM board and the Sivers IMA 60 GHz WiGig transceiver, the ZCU111 board also supports multi-tile synchronization (MTS) of the RF data-converter Xilinx IP. The RFSoC reads signals either in baseband or in RF utilizing a numerically controlled oscillator (NCO) to downconvert them and generate the corresponding baseband I/Q waveforms. While the base sampling rate is at 3,932.16 MHz in the MTS mode, the internal interpolation/decimation structure can be explored to reduce the bandwidth if needed.

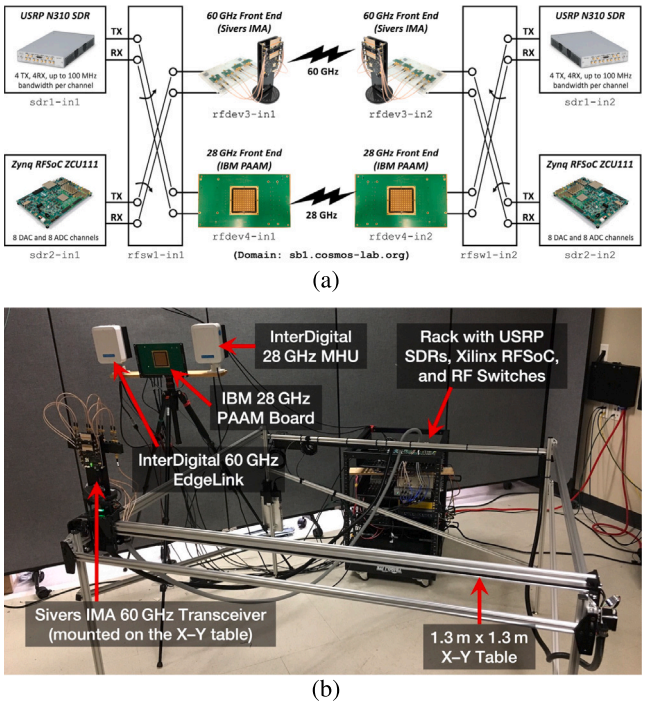

Fig. 5. The COSMOS Sandbox 1 (sb1): (a) block diagram of the bench-top mmWave setup with programmable 28/60 GHz front end systems, customized RF switches, USRP SDRs, and Xilinx RFSoC boards, and (b) view of a corner of sb1 in an indoor environment.

4.5. 28/60 GHz SDRs in the sandboxes (sb1 and sb2)

The key programmable mmWave radios in the COSMOS sb1 is a set of 28/60 GHz SDRs, each composed of a 28/60 GHz front end and a baseband platform. Fig. 5(a) depicts the block diagram of two sets of 28/60 GHz SDRs deployed in the two corners (in1 and in2) diagonally across the room, which has a dimension of 20 m×20 m×3 m (L×W×H). Fig. 5(b) shows the view of one corner of the room, which includes an IBM 28 GHz PAAM subsystem board and a Sivers IMA 60 GHz transceiver mounted on an X-Y positioning table (described later), which are connected to USRP SDRs or Xilinx RFSoC boards through a customized RF switch box. The COSMOS sb1 also includes the InterDigital 5G NR platform and EdgeLink radios, as shown in Figs. 1(b) and 5(b). In particular, the 5G NR platform is an NR Rel-15 28 GHz radio with a 64-element phased array and a Xilinx MPSoC-based processing unit in the baseband. EdgeLink is a 60 GHz wireless link solution based on the IEEE 802.11ad standard, which supports mmWave mesh transport technology with centrally controlled mesh software. Detailed information about these end-to-end mmWave systems and example tutorials can be found at [19].

The COSMOS sb1 also includes an X-Y table, which currently mounts the Sivers IMA 60 GHz transceiver (see Fig. 5(b)). The X-Y table allows for independent movement of each mmWave front end in the horizontal plane within a 1.3 m×1.3 m area, and rotating the arrays within ±45° about their vertical axis. This X-Y table has a positioning and rotational of 0.56 mm and 1 degree, respectively. Fig. 6 shows a customized JavaScript-based web interface for controlling the position and angle of the mounted arrays, which embeds the live camera streaming functionality so that users can monitor the X-Y table remotely. Depending on the research requirements, different mmWave front ends can be replaced to be mounted on the X-Y table.

Another COSMOS sandbox, sb2, is located in an indoor environment in the CEPSR building at Columbia University. In addition to sub-6 GHz SDRs and open-access full-duplex radios [23], sb2 currently houses two

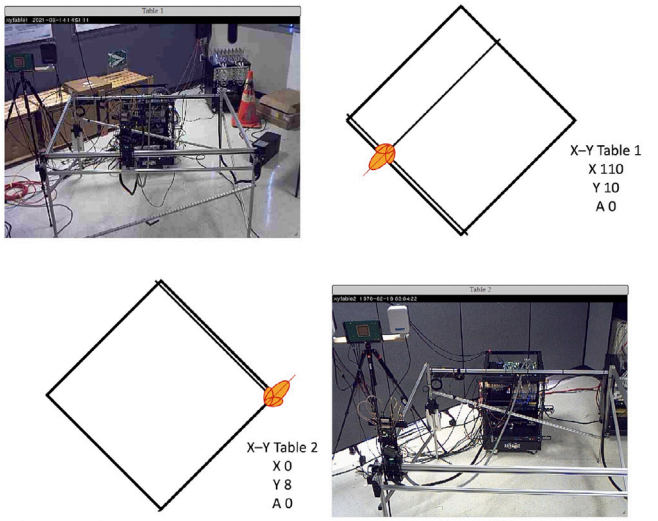

Fig. 6. Web interface (including live camera streaming) for controlling the X-Y table in sb1, on which mmWave front ends are mounted.

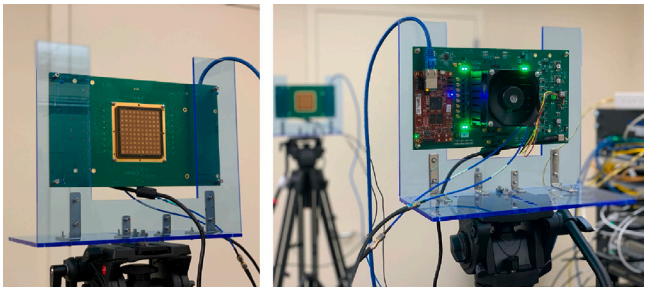

Fig. 7. Two 28 GHz PAAM subsystem boards integrated in COSMOS sb2 (SDRs and compute servers are not shown in the figure).

28 GHz SDRs, each integrated using a 28 GHz PAAM subsystem board and a USRP N310 SDR, as shown in Fig. 7. The USRP SDRs are connected to the data switch and compute servers located in the Computing Research Facilities (CRF) at Columbia University's Computer Science building via 10 GbE links. In Section 5.4, we present a real-time channel sounding experiment using the two 28 GHz SDRs deployed in sb2.

4.6. 28 GHz SDRs in the outdoor testbed (bed)

Fig. 8 depicts the location of the deployed COSMOS Sandbox2 (sb2), two large nodes (lg1–lg2), and four medium nodes (md1–md4) within an FCC Innovation Zone in West Harlem, NYC, and six more medium nodes (md6–md10) will also be deployed in the future. Each of the medium nodes, including the ones already deployed and to be deployed, is equipped with two 28 GHz PAAM subsystem boards. Fig. 9 shows the outdoor deployment of two medium nodes in the main outdoor testbed of COSMOS (bed) on the CCNY campus. In particular, one medium node (md3) is mounted on the side wall of the North Academic Center (NAC) building located at Amsterdam Avenue & West 136th Street, and the other medium node (md4) is mounted on top of a security guard booth located at Convent Avenue & West 133rd Street. The outdoor enclosure of each medium node includes two IBM 28 GHz PAAM subsystem boards, each covering a field-of-view (FoV) of 120°, four sub-6 GHz omnidirectional antennas and one GPS antenna (in the top radome), and two Power over Ethernet (PoE) cameras. The sub-6 GHz antennas and IBM 28 GHz PAAM subsystem boards are connected via coax cables to the USRP SDRs, which are then connected to compute servers located in the CCNY data center via 10 GbE links. The other two

Fig. 8. Location of the deployed COSMOS Sandbox2 (sb2), two large nodes (lg1–lg2), and four medium nodes (md1–md4) within an FCC Innovation Zone in West Harlem, NYC, with six more medium nodes (md6–md10) that will be deployed in the future.

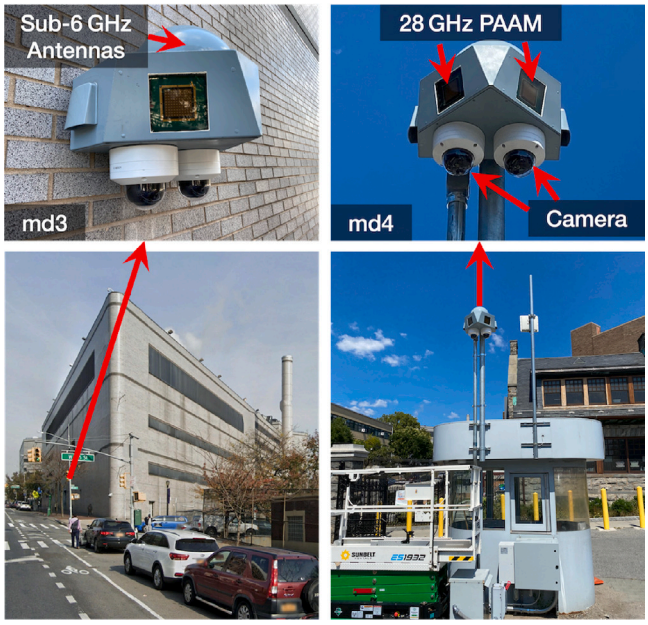

Fig. 9. The outdoor deployment of two COSMOS medium nodes (md3 and md4) on the CCNY campus, one on the side wall of the NAC building and one on the top of a security guard booth, each with two 28 GHz PAAM subsystem boards.

medium nodes (md1 and md2) deployed on the Columbia campus [11] will also be upgraded to include the IBM 28 GHz PAAM subsystem boards in an identical configuration as md3 and md4.

4.7. Mobile 28 GHz SDRs

To support experiments in mobile scenarios within the COSMOS testbed area (in both indoor and outdoor environments), we also build a mobile 28 GHz SDR using the PAAM subsystem board described in Section 4.1 and [14]. Fig. 10 shows the waterproof enclosure and internals of the mobile 28 GHz SDR, which includes a 28 GHz PAAM subsystem board and a USRP 2974 SDR. The USRP 2974 SDR can be controlled from the embedded PC and is equipped with 2 TX and 2 RX ports, which are connected to the TX-H/TX-V and RX-H/RX-V IF

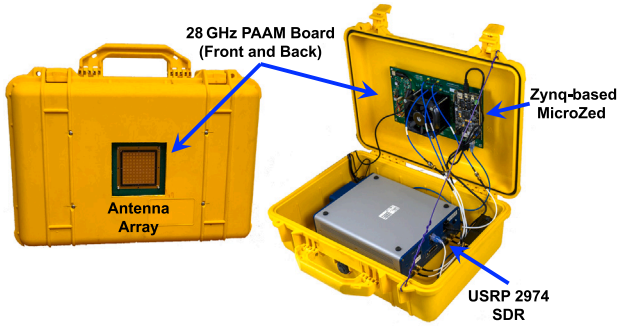

Fig. 10. A programmable mobile 28 GHz SDR using the PAAM board: the waterproof enclosure and internal component layout.

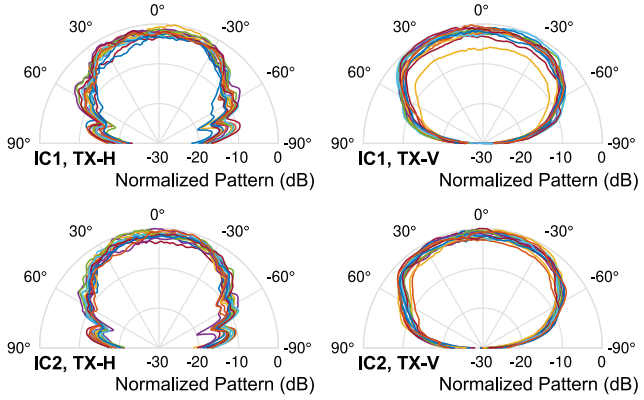

Fig. 11. Normalized individual TX element radiation pattern of two ICs (IC1 and IC2) of a 28 GHz PAAM subsystem board, in both H- and V-polarization, measured in an anechoic chamber.

ports of the 28 GHz PAAM subsystem board, respectively, and supports a real-time RF bandwidth of up to 200 MHz via the 10 GbE interface. Using such a capability, researchers can perform various experiments in mobile scenarios, where a user moving on the street (i.e., the compact mobile 28 GHz SDR) communicates with a fixed infrastructure node (e.g., a medium node equipped with the 28 GHz PAAM subsystem board). In future work, we will consider replacing the USRP 2974 SDR with a USRP X410 SDR or a Xilinx RFSoC board, which can support 4 TX-RX pairs with significantly enhanced real-time bandwidth.

5. Experimentation with the 28 GHz PAAM board

In this section, we present extensive measurements and an example channel sounding experiment using the 28 GHz PAAM subsystem boards integrated in the COSMOS sb1 and sb2.

5.1. Element radiation and beamforming pattern measurements

We first use an anechoic chamber to measure the TX element radiation patterns and array beamforming patterns. In particular, a 28 GHz PAAM subsystem board and a 28 GHz horn antenna are mounted on a rotational gimbal and a fixed pole, respective, which are separated by 1.5 m. A continuous wave (CW) signal at 3 GHz is generated by a Keysight signal generator and fed into the IF TX input port of each IC of the PAAM, and the received signal power at the horn antenna is recorded by a Keysight spectrum analyzer. Fig. 11 shows the normalized individual TX element radiation pattern measurements of IC1 and IC2 of a 28 GHz PAAM subsystem board, in both H- and V-polarization, where each front end element of an IC is individually activated using the PAAM API, described in Section 4.1. The overall results match with

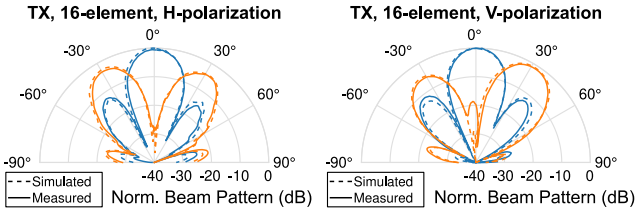

Fig. 12. Normalized TX beam patterns using one 16-element IC of a 28 GHz PAAM, with conventional beamforming that generates a single beam in the broadside ($\theta_{TX} = 0°$, blue), and arbitrary beamforming that simultaneously generates two beams in two directions ($\theta_{TX} = \pm 30°$, orange). (For interpretation of the references to color in this figure legend, the reader is referred to the web version of this article.)

those reported in [16], and show a small variation in the individual element radiation pattern in the array broadside.

We also characterize the TX beam pattern using the same setup in the anechoic chamber and focus on 16-element beams generated by an IC. We consider two types of beamforming: (*i*) conventional beamforming that generates a single TX beam in the array broadside ($\theta_{TX} = 0°$) using the PAAM API, and (*ii*) arbitrary beamforming that generates two simultaneous beams in the directions of $\theta_{TX} = \pm 30°$ with different beamforming gains. Fig. 12 shows the measured normalized TX beam patterns (solid lines) in both the H- and V-polarization, which very closely match with the simulated "ideal" beam patterns (dashed lines) due to the calibration-free nature of the 28 GHz PAAM. In addition, a peak-to-null ratio of more than 25 dB can be achieved using only 16 elements in a 4×4 planar array. All these measurement datasets are made available on the COSMOS wiki [18] and shared with the community.

5.2. TX and RX beamforming with SDRs

Next, we experiment with TX/RX beamforming capabilities of the 28 GHz PAAM subsystem boards integrated with SDRs, where the IF TX/RX ports in both the H-polarization and V-polarization on IC0 of a PAAM subsystem board are connected to two transceiver pairs on the N310 SDR (RF2 and RF3). We choose to use only one IC on the PAAM (IC0) with up to 16 front end elements, due to the short link distances of up to 70 ft in sb1. The outdoor deployment of the 28 GHz subsystem boards in bed (see Section 4.6) supports up to 64-element dual-polarized beamforming using all the 4 ICs, which can result in a link distance of 100 s of meters. The experimental results can also be applied to the mobile 28 GHz SDR described in Section 4.7.

TX beamforming: Fig. 13(a) shows the experimental setup for TX beamforming performance measurement, where the TX is a 28 GHz PAAM board integrated with a USRP N310 (PAAM1 and SDR1), and the RX is an SAS-588 standard gain horn antenna connected to a Keysight N9030 A PXA signal analyzer. The PAAM board and RX horn antenna, which face each other (roughly) in the broadside, are mounted on two tripods with the same height and the link distance between them is ~7 m. In particular, the N310 SDR generates a 100 kHz continuous wave (CW) at 3 GHz operating frequency and sends it to the IF TX input port of IC0 on the PAAM board, in the H-polarization or V-polarization. The PXA signal analyzer is configured with a center frequency of 28 GHz and a resolution bandwidth (RBW) of 10 kHz in order to capture received signal with low power levels, and the average received signal power is recorded. We perform measurements of the TX beamforming performance of the PAAM in both the H- and V-polarization, where the RX horn antenna is set up such that its polarization matches with that of the TX PAAM (PAAM1).

Figs. 13(b) and 13(c) show the measured received signal power as a function of the TX beam steering angle in the H- and V-polarization, respectively. In general, the TX beamforming performance is largely

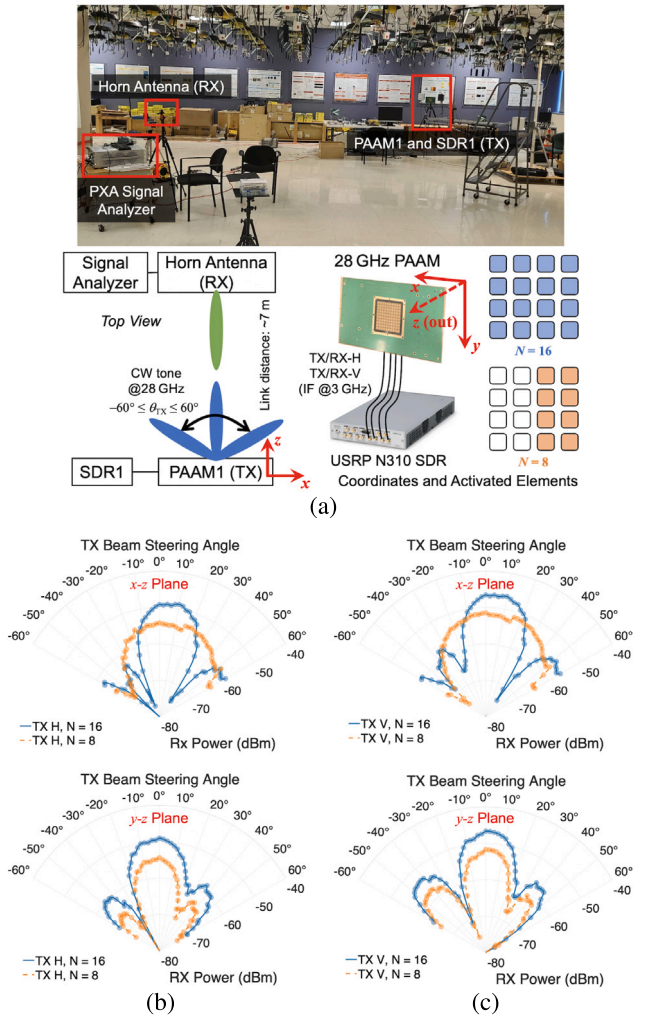

Fig. 13. (a) Setup for the TX beamforming measurements using the 28 GHz PAAM subsystem board in COSMOS sb1, which include a 28 GHz PAAM board, a USRP N310 SDR, a standard gain horn antenna, and a Keysight PXA signal analyzer. (b)–(c) Measured received signal power at the horn antenna with varying TX beam steering angles at the PAAM in the x–z and y–z plane, and in H- and V-polarization.

similar between the H- and V-polarization. For each polarization, the received signal power at the horn antenna is measured when the TX beam is swept across the x–z or y–z plane (see Fig. 13(a) for the coordinate system of the PAAM subsystem board), with 8 or 16 front end elements activated on IC0. The results show a clear beam shape as the TX beam is electronically steered using the developed PAAM API. With 16 antenna elements, a peak-to-null radio of >30 dB and an average half-power beamwidth of 26° are measured in the indoor environment of sb1. With only 8 front end elements activated on IC0, the peak received signal power is reduced by ~6 dB compared with the case with 16 front end elements, which is as expected. In addition, the half-power beamwidths on the x–z and y–z planes exhibit a large difference, due to the asymmetric number of elements on the x and y axes when 8 front end elements are activated. Note that these results *do not* show the standard TX beam pattern measurements, since the PAAM or the RX horn antenna is not mechanically rotated for each fixed TX beamforming direction.[1] However, the reported measurements are still valuable as a demonstration of the practical remote usage of

[1] The detailed setup and measurement results of the true TX/RX beam patterns in an antenna chamber are presented in [15].

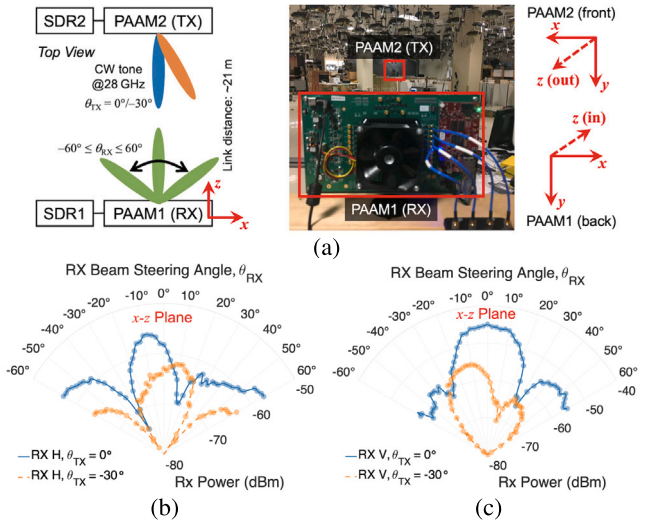

Fig. 14. (a) Setup for the RX beamforming measurements in COSMOS sb1, which includes two 28 GHz PAAM boards and two USRP N310 SDRs. (b)–(c) Measured received signal power with varying RX beam steering angles on the x–z plane in H- and V-polarization.

various hardware and software resources in sb1 with over-the-air signal transmissions.

RX beamforming: We conduct RX beamforming performance measurements using experimental setup shown in Fig. 14(a), where PAAM1 used in the TX beamforming measurements, described above, is configured in the RX mode, and another PAAM board with a USRP N310 (PAAM2 and SDR2) is used as the TX. On the TX side, we configure PAAM2 to form a 16-element TX beam in two directions (θ_{TX} = 0° and −30°) on the x–z plane, and SDR2 to generate a 100 kHz CW at 3 GHz carrier frequency, which is sent to the IF TX input port of IC0 on PAAM2. On the RX side, PAAM1 is configured to form a 16-element RX beam in the x–z plane, and the received signal power at SDR1 as PAAM1 sweeps across varying RX beamforming directions is recorded.

Figs. 14(b) and 14(c) show the measured received signal power as a function of the RX beam steering angle, θ_{RX}, in the H- and V-polarization, respectively. The results show that the maximum received signal power in the V-polarization is ~10 dB higher than that achieved in the H-polarization in the sb1 indoor environment. This is due to the spatial dimension of sb1, which is an indoor environment with a dimension of 20 m×20 m×3 m (L×W×H), as shown in Figs. 13(a) and 14(a). When the signal propagates on the y–z plane (V-polarization), its energy is "trapped" between the ceiling and ground on the indoor environment, resulting in a higher RX power level compared with the H-polarization. Similar effects stemming from the sb1 indoor environment can also be seen by the strong RX signal power in the H-polarization at $\theta_{RX} = \pm 60°$ on the x–z plane. In practice, a smaller number of front end elements (e.g., 4 or 8) on the TX and RX side can already form a link with a sufficient signal-to-noise ratio (SNR) at ~70 feet distance. However, we perform measurements using 16-element TX and RX beams with a narrower half-power beamwidth in order to quantify the spatial distribution of the RX signal power.

5.3. Timing of the PAAM API functions

We now evaluate the timing of the main IC-level PAAM functions, described in Table 1, using the same setup shown in Fig. 14(a), and the main results are summarized in Table 2.

Beam steering and switching: To experimentally measure the beam steering/switching time, we configure PAAM1 (RX) to form a 16-element RX beam in the broadside, and configure PAAM2 (TX) to

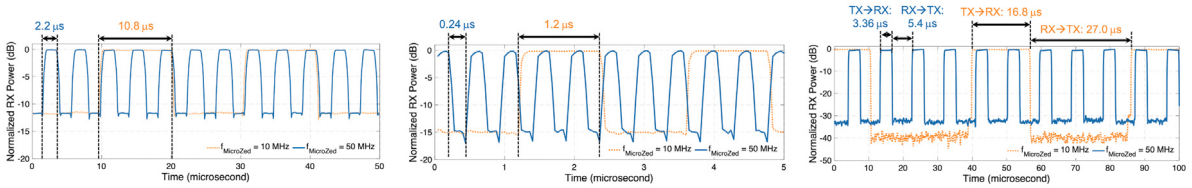

(a) The steer_beam() function (b) The switch_beam_index() function (c) TX-RX switching

Fig. 15. (a)–(b) Measured time to switch between two TX beams on the x–z plane ($\theta_{TX} = 0°$ and 30°), and (c) measured time to switch between the TX and RX modes using 16 front end elements of an IC on the PAAM.

Table 2
Timing of the IC-level functions supported by the PAAM board and software API using a single IC. Details of each function can be found in Table 1.

PAAM API command	$f_{\text{MicroZed}} = 10$ MHz	$f_{\text{MicroZed}} = 50$ MHz
enable()[a]	<28.2 µs	<5.64 µs
steer_beam()[a]	<40.8 µs	<8.16 µs
set_arbitrary_beam()[a]	<40.8 µs	<8.16 µs
switch_beam_index()	2.4 µs	0.48 µs
switch_beam_indexes()	2.4 µs	0.48 µs

[a]Running time depends on the number of used front end elements.

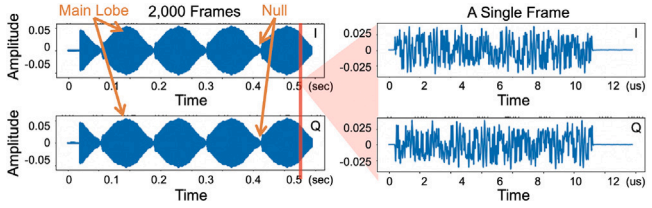

Fig. 16. Baseband I/Q waveforms of a real-time 28 GHz SISO channel sounding demonstration with TX beam switching.

generate a 16-element TX beam and continuously switch between two TX beamforming directions, $\theta_{TX} = 0°$ and 30°. Figs. 15(a) and 15(b) show the received signal power at PAAM1 when PAAM2 employs the steer_beam() and switch_beam_index() functions, respectively. The results show that by computing and storing the beamforming codebook in advance, the switch_beam_index() function improves the beam switching time by a factor of 10× compared to the steer_beam() function, which computes the codebook every time a beamforming direction is given. Overall, with a MicroZed frequency of 50 MHz, the switch_beam_index() function enables extremely fast beam switching at a speed of only 0.24 µs. This duration is much shorter than the OFDM symbol duration for 5G NR in the frequency range 2 (FR2), which is usually at the order of 10 s of µs. Note that this time duration is shorter than that described in Table 2, since few API commands are needed to execute the experiment. As a result, the PAAM board can support symbol-level beam switching for practical 28 GHz systems. Moreover, here we report the command execution time on the MicroZed, which excludes the host-to-MicroZed latency (which is ~0.1 ms in sb1 and sb2). However, this can be resolved by pre-recording and replaying long sequences of commands in the Microzed.

TX-RX switching: Using a similar approach, we perform measurements to characterize the timing of the TX-RX switching operation using the PAAM (i.e., switching from TX mode to RX mode, or vice versa), which is a critical functionality for many time division duplexing (TDD) systems. In particular, we configure PAAM2 to continuously switch between TX and RX mode with all the 16 elements on IC0 enabled, where each switching operation is realized using two functions executed in sequential order: enable(), which enables the TX/RX mode, followed by switch_beam_index(), which sets the TX/RX beamforming direction. On the other side, we configure PAAM1 to form a fixed 16-element RX beam in the broadside. Fig. 15(c) shows the average received signal power at PAAM1 as a function of time, from which the TX-RX switching, performed at PAAM2, can be observed. The results show that at the maximum MicroZed clock frequency of 50 MHz, the duration to perform a TX→RX and RX→TX switching operation is 3.36 µs and 5.40 µs, respectively. Since the switch_beam_index() function takes a minimum amount of time (i.e., only 0.24 us as shown in Fig. 15(b)), the major timing overhead during a TX-RX switching operation results from the execution of the enable() function, which increases as more front end elements need to be switched on/off and is different for TX and RX modes. Similar to the case of beam steering and switching, this TX-RX switching time is shorter than that described in Table 2, since few API commands are needed to execute the experiment.

5.4. A 28 GHz channel sounding experiment

We also present a 28 GHz channel sounding experiment using two PAAM boards integrated with N310 SDRs in sb2, with a real-time bandwidth of 62.5 MHz. In particular, we configure one PAAM board and an N310 SDR to emulate a client, which generates an 8-element beam in the broadside in the H-polarization, and continuously sends a known sounding pilot sequence on the uplink. We configure the other PAAM board and an N310 SDR to emulate a base station, which continuously sweeps an 8-element RX beam on its x–z plane within $\theta_{RX} \in [-30°, 30°]$ in the H-polarization, using the steer_beam_index() method running at 2 ms time interval. The software for this experiment is built on the open-source C++-based RENEW channel sounder [44], which we have enhanced to support UHD-based SDRs. Fig. 16 shows the baseband I/Q waveforms of the uplink pilot received at the base station, where the amplitude of the RX signal varies in proportion to the RX beam steering directions. Further channel sounding information can be obtained by analyzing the I/Q waveforms, and the details can be found in [19]. More advanced mmWave experiments using the PAAM boards are under development and will be made open-source once available.

6. Experimentation with the Sivers 60 GHz transceiver

CIR Computation using the IEEE 802.11ad Preamble:

We first present an experiment that uses RFNoC blocks to obtain the real-time channel impulse response (CIR) at 60 GHz using the IEEE 802.11adpreamble. Fig. 17(a) shows the GNU Radio flowgraph consisting of several RFNoC blocks including packet detector, carrier frequency offset (CFO) estimation and correction, symbol timing estimator, and frame boundary detector. These blocks were developed by IMDEA Networks Institute for the EU ORCA project [45]. We use the Sivers IMA 60 GHz front end transceivers integrated with USRP N310 SDRs in sb1 (see Fig. 5) and two host servers to control the Sivers transceivers and execute the GNU Radio RFNoC flowgraph. Pre-generated 802.11ad frames are repeatedly streamed from the TX N310, and the real-time CIR is obtained at the RX N310 that runs the 802.11ad preamble flowgraph. Figs. 17(b) and 17(c) show the magnitude of the CIR with two different TX beam steering angles. In particular, the RFNoC blocks compute the cross-correlation of the received channel estimation field of the preamble with a local known sequence with an

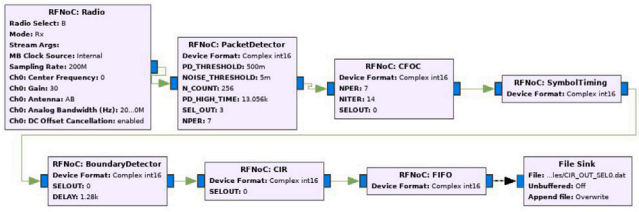

(a) Receive GRC flowgraph for CIR computation

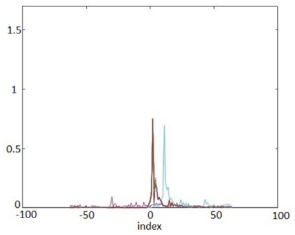

(b) CIR with TX beam angle 0°

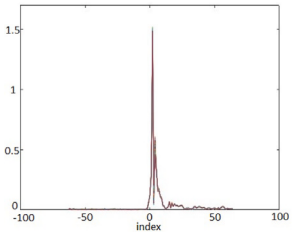

(c) CIR with TX beam angle −5°

Fig. 17. An example experiment on RFNoC-based 802.11ad preamble processing in COSMOS sb1.

offset between [−63, 64], and an offset with index 0 corresponding to the line-of-sight direct path between the TX and RX.

Over-the-Air Transmission using the Xilinx RFSoC: We also developed an example experiment with over-the-air signal transmission using the RFSoC board with the Sivers IMA 60 GHz front end transceivers in sb1. Using the developed non-real-time library and API described in Section 4.4, users can send data to the DACs, receive data from the ADCs, and configure the operating frequency and TX/RX beam steering directions. The received and stored data can then be processed in an online or offline manner. The detailed tutorial can be found in [19].

7. Conclusion

In this paper, we presented the design and implementation of programmable and open-access mmWave radios based on the IBM 28 GHz PAAM subsystem board and the Sivers IMA 60 GHz transceiver system. We also presented their integration in the COSMOS testbed in both indoor and outdoor environments, as well as the associated measurements and experimentation. Our ongoing development efforts include more advanced software (both host- and FPGA-based) for mmWave experiments at different networking layers, and the support of mmWave MIMO communication. We believe that these capabilities supported by COSMOS' programmable mmWave radios can enable a wide range of complex mmWave experiments in both static and mobile scenarios.

CRediT authorship contribution statement

Tingjun Chen: Methodology, Data curation, Software, Investigation, Validation, Visualization, Writing – original draft, Writing – review & editing, Funding acquisition. **Prasanthi Maddala:** Data curation, Software. **Panagiotis Skrimponis:** Data curation, Software. **Jakub Kolodziejski:** Methodology, Software. **Abhishek Adhikari:** Data curation. **Hang Hu:** Data curation. **Zhihui Gao:** Data curation. **Arun Paidimarri:** Software, Writing – review & editing. **Alberto Valdes-Garcia:** Writing – review & editing, Supervision. **Myung Lee:** Writing – review & editing. **Sundeep Rangan:** Methodology, Writing – review & editing. **Gil Zussman:** Conceptualization, Methodology, Writing – review & editing, Funding acquisition, Supervision. **Ivan Seskar:** Conceptualization, Methodology, Funding acquisition, Supervision.

Declaration of competing interest

The authors declare that they have no known competing financial interests or personal relationships that could have appeared to influence the work reported in this paper.

Data availability

Most of the tutorial, data, and source code are made available at https://wiki.cosmos-lab.org/wiki/.

Acknowledgments

This work was supported in part by the National Science Foundation (NSF), United States grants CNS-1827923, OAC-2029295, EEC-2133516, CNS-2211944, AST-2232455, AST-2232458, and AST-2232459, an IBM Academic Award, United States, and the industrial affiliates of NYU WIRELESS, United States. This work was also supported in part by NSF, United States grant CNS-2148128 and by funds from federal agency and industry partners as specified in the Resilient & Intelligent NextG Systems (RINGS) program, United States, and in part by the Center for Ubiquitous Connectivity (CUbiC), United States, sponsored by Semiconductor Research Corporation (SRC), United States and Defense Advanced Research Projects Agency (DARPA), United States under the JUMP 2.0 program. We also thank Xiaoxiong Gu, Bodhisatwa Sadhu, and Stanislav Lukashov from IBM Research for their contributions to this project.

References

[1] Theodore S Rappaport, Shu Sun, Rimma Mayzus, Hang Zhao, Yaniv Azar, Kevin Wang, George N Wong, Jocelyn K Schulz, Mathew Samimi, Felix Gutierrez, Millimeter-wave mobile communications for 5G cellular: It will work! IEEE Access 1 (2013) 335–349.

[2] Sundeep Rangan, Theodore S. Rappaport, Elza Erkip, Millimeter-wave cellular wireless networks: Potentials and challenges, Proc. IEEE 102 (3) (2014) 366–385.

[3] Thomas Nitsche, Carlos Cordeiro, Adriana B Flores, Edward W Knightly, Eldad Perahia, Joerg C Widmer, IEEE 802.11ad: directional 60GHz communication for multi-Gigabit-per-second Wi-Fi, IEEE Commun. Mag. 52 (12) (2014).

[4] Marco Giordani, Michele Polese, Marco Mezzavilla, Sundeep Rangan, Michele Zorzi, Toward 6G networks: Use cases and technologies, IEEE Commun. Mag. 58 (3) (2020) 55–61.

[5] Swetank Kumar Saha, Yasaman Ghasempour, Muhammad Kumail Haider, Tariq Siddiqui, Paulo De Melo, Neerad Somanchi, Luke Zakrajsek, Arjun Singh, Roshan Shyamsunder, Owen Torres, et al., X60: A programmable testbed for wideband 60 GHz WLANs with phased arrays, Comput. Commun. 133 (2019) 77–88.

[6] Renjie Zhao, Timothy Woodford, Teng Wei, Kun Qian, Xinyu Zhang, M-Cube: A millimeter-wave massive MIMO software radio, in: Proc. ACM MobiCom'20, 2020.

[7] Jesus Omar Lacruz, Dolores Garcia, Pablo Jiménez Mateo, Joan Palacios, Joerg Widmer, mm-FLEX: an open platform for millimeter-wave mobile full-bandwidth experimentation, in: Proc. ACM MobiSys'20, 2020.

[8] Jesus Lacruz, Rafael Ortiz, Joerg Widmer, A real-time experimentation platform for sub-6 GHz and millimeter-wave MIMO systems, in: Proc. ACM MobiSys'21, 2021.

[9] Jialiang Zhang, Xinyu Zhang, Pushkar Kulkarni, Parameswaran Ramanathan, OpenMili: A 60 GHz software radio platform with a reconfigurable phased-array antenna, in: Proc. ACM MobiCom'16, 2016.

[10] Omid Abari, Haitham Hassanieh, Michael Rodreguiz, Dina Katabi, Poster: A millimeter wave software defined radio platform with phased arrays, in: Proc. ACM MobiCom'16, 2016.

[11] Dipankar Raychaudhuri, Ivan Seskar, Gil Zussman, Thanasis Korakis, Dan Kilper, Tingjun Chen, Jakub Kolodziejski, Michael Sherman, Zoran Kostic, Xiaoxiong Gu, Harish Krishnaswamy, Sumit Maheshwari, Panagiotis Skrimponis, Craig Gutterman, Challenge: COSMOS: A city-scale programmable testbed for experimentation with advanced wireless, in: Proc. ACM MobiCom'20, 2020.

[12] Platforms for advanced wireless research (PAWR), 2021, https://www.advancedwireless.org/.

[13] Tingjun Chen, Prasanthi Maddala, Panagiotis Skrimponis, Jakub Kolodziejski, Xiaoxiong Gu, Arun Paidimarri, Sundeep Rangan, Gil Zussman, Ivan Seskar, Programmable and open-access millimeter-wave radios in the PAWR COSMOS testbed, in: Proc. ACM WiNTECH'21, 2022.

[14] Xiaoxiong Gu, Arun Paidimarri, Bodhisatwa Sadhu, Christian Baks, Stanislav Lukashov, Mark Yeck, Young Kwark, Tingjun Chen, Gil Zussman, Ivan Seskar, Alberto Valdes-Garcia, Development of a compact 28-GHz software-defined phased array for a city-scale wireless research testbed, in: Proc. IEEE IMS'21, 2021.

[15] Bodhisatwa Sadhu, Yahya Tousi, Joakim Hallin, Stefan Sahl, Scott K Reynolds, Örjan Renström, Kristoffer Sjögren, Olov Haapalahti, Nadav Mazor, Bo Bokinge, et al., A 28-GHz 32-element TRX phased-array IC with concurrent dual-polarized operation and orthogonal phase and gain control for 5G communications, IEEE J. Solid-State Circuits 52 (12) (2017) 3373–3391.

[16] Xiaoxiong Gu, Duixian Liu, Christian Baks, Ola Tageman, Bodhisatwa Sadhu, Joakim Hallin, Leonard Rexberg, Pritish Parida, Young Kwark, Alberto Valdes-Garcia, Development, implementation, and characterization of a 64-element dual-polarized phased-array antenna module for 28-GHz high-speed data communications, IEEE Trans. Microw. Theory Tech. 67 (7) (2019) 2975–2984.

[17] Innovation zones for program experimental licenses in designated portions of New York City and Salt Lake City, 2019, https://docs.fcc.gov/public/attachments/DA-19-923A1.pdf/.

[18] COSMOS wiki, 2023, https://wiki.cosmos-lab.org/wiki/.

[19] COSMOS tutorials, 2023, https://wiki.cosmos-lab.org/wiki/tutorials/.

[20] Prasad Netalkar, Azhaan Zahabee, Carlos E Caicedo Bastidas, Igor Kadota, Dragoslav Stojadinovic, Gil Zussman, Ivan Seskar, Dipankar Raychaudhuri, Large-scale dynamic spectrum access with IEEE 1900.5.2 spectrum consumption models, in: Proc. IEEE WCNC'23, 2023.

[21] Imtiaz Nasim, Panagiotis Skrimponis, Ahmed S Ibrahim, Sundeep Rangan, Ivan Seskar, Reinforcement learning of millimeter wave beamforming tracking over COSMOS platform, in: Proc. ACM WiNTECH'22, 2022.

[22] Tingjun Chen, Mahmood Baraani Dastjerdi, Jin Zhou, Harish Krishnaswamy, Gil Zussman, Wideband full-duplex wireless via frequency-domain equalization: Design and experimentation, in: Proc. ACM MobiCom'19, 2019.

[23] Manav Kohli, Tingjun Chen, Mahmood Baraani Dastjerdi, Jackson Welles, Ivan Seskar, Harish Krishnaswamy, Gil Zussman, Open-access full-duplex wireless in the ORBIT and COSMOS testbeds, in: Proc. ACM WiNTECH'20, 2020.

[24] Jinfeng Du, Dmitry Chizhik, Reinaldo A Valenzuela, Rodolfo Feick, Guillermo Castro, Mauricio Rodriguez, Tingjun Chen, Manav Kohli, Gil Zussman, Directional measurements in urban street canyons from macro rooftop sites at 28 GHz for 90% outdoor coverage, IEEE Trans. Antennas Propag. 69 (6) (2020) 3459–3469.

[25] Lars Grannemann, Aleksandar Ichkov, Petri Mähönen, Ljiljana Simić, Urban outdoor measurement study of phased antenna array impact on millimeter-wave link opportunities and beam misalignment, IEEE Trans. Wirel. Commun. 20 (3) (2020) 1727–1741.

[26] Anfu Zhou, Xinyu Zhang, Huadong Ma, Beam-forecast: Facilitating mobile 60GHz networks via model-driven beam steering, in: Proc IEEE INFOCOM'17, 2017.

[27] Ding Zhang, Mihir Garude, Parth H. Pathak, mmChoir: Exploiting joint transmissions for reliable 60GHz mmWave WLANs, in: Proc. ACM MobiHoc'18, 2018.

[28] Sanjib Sur, Ioannis Pefkianakis, Xinyu Zhang, Kyu-Han Kim, Towards scalable and ubiquitous millimeter-wave wireless networks, in: Proc. ACM MobiCom'18, 2018.

[29] Omid Abari, Dinesh Bharadia, Austin Duffield, Dina Katabi, Enabling high-quality untethered virtual reality, in: Proc. USENIX NSDI'17, 2017.

[30] Suraj Jog, Jiaming Wang, Junfeng Guan, Thomas Moon, Haitham Hassanieh, Romit Roy Choudhury, Many-to-many beam alignment in millimeter wave networks, in: Proc. USENIX NSDI'19, 2019.

[31] Aleksandar Ichkov, Simon Häger, Petri Mähönen, Ljiljana Simić, Comparative evaluation of millimeter-wave beamsteering algorithms using outdoor phased antenna array measurements, in: Proc. IEEE SECON'22, IEEE, 2022.

[32] A Lee Swindlehurst, Ender Ayanoglu, Payam Heydari, Filippo Capolino, Millimeter-wave massive MIMO: The next wireless revolution? IEEE Commun. Mag. 52 (9) (2014) 56–62.

[33] Yasaman Ghasempour, Muhammad K Haider, Carlos Cordeiro, Dimitrios Koutsonikolas, Edward Knightly, Multi-stream beam-training for mmwave MIMO networks, in: Proc. ACM MobiCom'18, 2018.

[34] Aditya Dhananjay, Kai Zheng, Marco Mezzavilla, Dennis Shasha, Sundeep Rangan, Fully-digital beamforming demonstration with Pi-Radio mmWave SDR platform, in: Proc. ACM MobiHoc'20, 2020.

[35] POWDER: Platform for open wireless data-driven experimental research, https://powderwireless.net/.

[36] RENEW: Reconfigurable eco-system for next-generation end-to-end wireless, https://renew.rice.edu/.

[37] AERPAW: Aerial experimentation and research platform for advanced wireless, https://aerpaw.org/.

[38] ARA: Wireless living lab for smart and connected rural communities, https://arawireless.org/.

[39] The Colosseum RF Emulator, https://www.northeastern.edu/colosseum/.

[40] Bodhisatwa Sadhu, Arun Paidimarri, Mark Ferriss, Mark Yeck, Xiaoxiong Gu, Alberto Valdes-Garcia, A 128-element dual-polarized software-defined phased array radio for mm-wave 5G experimentation, in: Proc. ACM MmNets'18, 2018.

[41] Tingjun Chen, Manav Kohli, Tianyi Dai, Angel Daniel Estigarribia, Dmitry Chizhik, Jinfeng Du, Rodolfo Feick, Reinaldo A Valenzuela, Gil Zussman, 28 GHz channel measurements in the COSMOS Testbed Deployment Area, in: Proc. ACM MmNets'19, 2019.

[42] Tingjun Chen, et al., A software-defined programmable testbed for beyond 5G optical-wireless experimentation at city-scale, IEEE Netw. 36 (2) (2022).

[43] Cloud enhanced open software defined mobile wireless testbed for city-scale deployment (COSMOS), 2023, https://cosmos-lab.org/.

[44] RENEWLab: An open-source software toolbox for the RENEW massive MIMO platform, 2021, https://github.com/renew-wireless/RENEWLab.

[45] ORCA MISO webpage, 2021, https://www.orca-project.eu/millimeter-wave-open-experimentation-platform/.

Tingjun Chen received the Ph.D. degree in electrical engineering from Columbia University in 2020, and the B. Eng. degree in electronic engineering from Tsinghua University in 2014. He is an Assistant Professor of Electrical and Computer Engineering at Duke University and was a postdoctoral associate at Yale University from 2020–2021. His research interests are in the area of networking and communications with a focus on next-generation wireless networks and Internet-of-Things systems. He received the Google Research Scholar Award, IBM Academic Award, Facebook Fellowship, and Columbia Engineering Morton B. Friedman Memorial Prize for Excellence. He also received the ACM CoNEXT'16 Best Paper Award and ACM SIGMOBILE Dissertation Award Runner-up.

Prasanthi Maddala is a research engineer at WINLAB, Rutgers University. After obtaining her Masters degree in Telecommunications from Indian Institute of Science, Bangalore, she joined WINLAB and worked on various projects involving SDR platforms, with her main focus on FPGA and embedded development. Her recent technical interests include SDR development for mmWave and wideband communication systems.

Panagiotis Skrimponis received the Diploma degree in computer, communication and network engineering and the M. Sc. degree in electrical and computer engineering from the University of Thessaly, Greece, in 2015 and 2018, respectively. From 2013 to 2018, he worked at the Center for Research and Technology Hellas (CERTH), EPFL, and New York University, as a Research Assistant. His research interests include prototyping systems using advanced FPGA/SoC platforms, develop communications systems using USRP and SDR devices, apply performance and power optimizations for mmWave and THz communication systems, and design interactive hands-on STEM learning experiences for K–12 students and teachers.

Jakub Kolodziejski is a project engineer at Rutgers WINLAB, specializing in wireless communications and research hardware development. He holds an MS in Computer and Electrical Engineering from Rutgers University, as well as BS degrees in Physics from Seton Hall University and Electrical and Computer Engineering from NJIT. With a keen interest in hardware prototyping, Jakub has actively contributed to collaborative projects such as the ORBIT and COSMOS testbeds. His expertise lies in bridging the gap between theory and practical implementation, driving advancements in wireless technologies.

Abhishek Adhikari received the B.S. degree in computer engineering (Magna Cum Laude) from Drexel University in 2021. He is currently an M.S./Ph.D. student in the Department of Electrical Engineering at Columbia University. His research is on wireless communication and sensing, with a focus on path loss modeling and micro-climate prediction using millimeter-wave. Abhishek was the recipient of the Evergreen Fellowship in 2021.

Hang Hu received the B.E. and M.S. degrees from Northeastern University, Shenyang, China, in 2015 and 2018, respectively. He is currently pursuing the Ph.D. degree with the Department of Electrical Engineering, The City College of New York, CUNY, New York, USA. His research interests include deep reinforcement learning for resource allocation and management, and machine learning for vehicle-to-everything (V2X) applications.

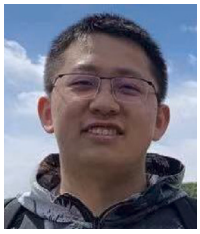

Zhihui Gao is a Ph.D. student in the Department of Electrical and Computer Engineering at Duke University. He received his B.Eng. degree in electrical engineering from Fudan University in 2020. His research interests include cyber–physical system (CPS) and the next-generation wireless networks.

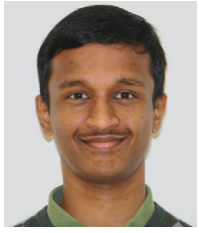

Arun Paidimarri received the B.Tech degree in electrical engineering from the Indian Institute of Technology, Bombay, India, and the S.M. and Ph.D degrees in electrical engineering and computer science from the Massachusetts Institute of Technology (MIT), Cambridge. He is currently a Senior Research Scientist at the IBM T.J. Watson Research Center, Yorktown Heights, NY. He is an Adjunct Assistant Professor at Columbia University, New York, NY. His research interests are in low power wireless system design, mm-wave circuit design and software-defined phased arrays. He is a member of the technical program committees for RFIC Symposium and BCICTS.

Alberto Valdes-Garcia received the Ph.D. degree in E.E. from Texas A&M University in 2006. He is currently Principal Research Scientist, Manager at the IBM T. J. Watson Research Center. In this role, he leads a multi-disciplinary team in the development of technologies that bridge the gap between antennas and AI, enabling new mmWave systems for sensing and communications. He holds >130 issued U.S. patents and has co-authored >140 peer-reviewed publications. In 2020–2021 he served as Chair of the IEEE MTT-S Microwave and Millimeter-wave Integrated Circuits Technical Committee and currently serves in the Editorial Board of the IEEE Journal of Microwaves.

Myung Jong Lee received a B.S and an M.S from Seoul National University in Korea and Ph.D. from Columbia University. He is a professor in the Department of Electrical Engineering and Computer Science at the City College Graduate Center, CUNY. His current research interests include deep learning for multi-resource management for mobile/edge cloud computing/wireless networks, secure V2X communications, stochastic computing, and wireless testbed. He has 25 U.S. and International patents. Dr. Lee served TG chairs, IEEE 802.15.8 (Peer Aware Communications) and IEEE 802.15.5 (WPAN Mesh), and received CUNY Performance Excellence Award.

Sundeep Rangan is a Professor of Electrical and Computer Engineering at New York University. In 2000, he co-founded (with four others) Flarion Technologies that developed the first cellular OFDM data system and pre-cursor to 4G cellular systems including LTE and WiMAX. In 2006, Flarion was acquired by Qualcomm Technologies, where he became a Senior Director of Engineering. He received his B.A.Sc at the University of Waterloo, Canada and the M.Sc. and Ph.D. at the University of California, Berkeley, all in Electrical Engineering.

Gil Zussman received the Ph.D. degree in Electrical Engineering from the Technion in 2004 and was a postdoctoral associate at MIT in 2004–2007. Since 2007 he been with Columbia University where he is a Professor of Electrical Engineering and Computer Science (affiliated). His research interests are in the areas of wireless, mobile, and resilient networks. He is the Columbia PI of the COSMOS project. He is an IEEE Fellow and recipient of the Fulbright Fellowship, the DTRA Young Investigator Award, two Marie Curie Fellowships, the NSF CAREER Award, and 7 paper awards.

Ivan Seskar is the Chief Technologist at WINLAB, Rutgers University, responsible for experimental systems. He is currently the program director for the COSMOS project responsible for the New York City NSF PAWR deployment. He has also been the co-PI and project manager for the NSF-supported ORBIT mid-scale testbed project, successfully leading technology development and operations since the testbed was released in 2005 and for which the team received the 2008 NSF Alexander Schwarzkopf Prize for Technological Innovation. Ivan is a co-chair of the IEEE INGR Testbed Working Group, member of the IEEE Standardization Programs Development Board, and the co-founder and CTO of Upside Wireless Inc.